Dual wavelength lidar observation of tropical high-altitude cirrus clouds during the ALBATROSS 1996 campaign

Georg Beyerle,[1,2] Jürgen Schäfer,[2,3] Roland Neuber,[2] Otto Schrems,[2] I. Stuart McDermid[1]

Short title: LIDAR OBSERVATIONS OF TROPICAL CIRRUS CLOUDS

[1]Jet Propulsion Laboratory, California Institute of Technology, Wrightwood, CA

[2]Alfred Wegener Institute for Polar and Marine Research, Bremerhaven and Potsdam, Germany

[3]now at Forschungszentrum Jülich, Germany

Abstract. Dual wavelength aerosol lidar observations of tropical high-altitude cirrus clouds were performed during the ALBATROSS 1996 campaign aboard the research vessel "POLARSTERN" on the Atlantic ocean in October–November 1996. On the basis of 57 hours of night-time observations between 23.5°N and 23.5°S we find in 72% of the altitude profiles indications of the presence of cirrus cloud layers. This percentage drops to 32% at subtropical latitudes (23.5°–30°) based on 15 hours of data. About one-half of the subtropical and tropical cirrus layers are subvisual with an optical depth of less than 0.03 at a wavelength of 532 nm. In general the clouds exhibit high spatial and temporal variability on scales of a few tens of meters vertically and a few hundred meters horizontally. No clouds are observed above the tropopause. An abrupt change in the relation between the color ratios of the parallel and perpendicular backscatter coefficients at about 240 K is interpreted in terms of changes of particle shape and/or size distribution. At temperatures between 195 and 255 K a small fraction of the observations are consistent with the presence of small particles with dimensions of less than 0.1 μm.

1. Introduction

The frequent occurrence of high-altitude cirrus clouds at tropical latitudes is well known from satellite observations [*Prabhakara et al.*, 1988; *Wang et al.*, 1994]. Because of their ubiquitous nature and global distribution these cloud layers can significantly affect the radiation budget of the atmosphere [e.g., *Stephens et al.*, 1990]. Furthermore, as tropospheric air enters the stratosphere predominantly in the tropics by upward transport the formation of tropical cirrus layers influences the stratospheric water vapour content [e.g., *Danielsen*, 1993; *Potter and Holton*, 1995]. Recently, interest in high-altitude cirrus clouds has focused on heterogeneous processing on cirrus ice particles leading to chlorine activation [*Borrmann et al.*, 1996; *Solomon et al.*, 1997].

In the following we present results from dual-wavelength lidar observations of tropical visible and subvisual cirrus clouds above the Atlantic ocean during the ALBATROSS campaign (Atmospheric chemistry and lidar studies above the Atlantic ocean related to ozone and other trace gases in the tropo- and stratosphere) in October–November 1996. The measurements were performed aboard the research vessel "POLARSTERN" during a cruise from Bremerhaven, Germany (53.6°N, 8.6°E) to Punta Quilla, Argentina (50.2°S, 68.3°W) in October–November 1996 between 35°N and 45°S latitude and 25°W and 30°W longitude. The purpose of this study is, first, to enhance the data set on the occurrence frequency of optical thin cirrus clouds in the tropics, second, to collect cirrus lidar data with high temporal and spatial resolution, and third, to study the wavelength dependence of aerosol backscatter coefficient as well as aerosol depolarization.

2. Instrumentation and data reduction

The aerosol Raman lidar instrument transmits simultaneously at wavelengths of $\lambda_1 = 355$ nm and $\lambda_2 = 532$ nm with a pulse repetition frequency of 30 Hz. Elastic

and inelastic components of the backscattered light due to molecular and aerosol scattering and due to vibrational Raman scattering on molecular nitrogen, respectively, at altitudes between 5 and 50 km are detected. Additionally, the instrument includes detection channels for cross-polarized return signals at 355 and 532 nm. During data acquisition detected signals are averaged over 1,000 (0.5 minutes) or 4,000 laser pulses (2.2 minutes). The instrument operated during night-time only. Further technical details can be found in *Schäfer et al.* [1995].

For data analysis the raw data are summed over 12,000 laser pulses and corrected for photodetector saturation, deadtime effects and background noise. In the following $\beta^{A,M}(z,\lambda)$ ($\alpha^{A,M}(z,\lambda)$) denotes the backscatter (extinction) coefficient for aerosol (superscript A) and molecular (superscript M) scattering as a function of altitude z and wavelength λ, respectively. Backscatter ratio $R_{\|} = \beta_{\|}^{A}/\beta_{\|}^{M} + 1$ is derived from the corrected elastic and inelastic return signals, $P_{\|}(z,\lambda)$ and $P(z,\lambda^R)$, by

$$R_{\|}(z) = K\,\frac{P_{\|}(z,\lambda)}{P(z,\lambda^R)}\,\exp\int_{z_s}^{z} d\tilde{z}\,\left(\alpha^M(\tilde{z},\lambda) - \alpha^M(\tilde{z},\lambda^R)\right). \qquad (1)$$

Here, $\lambda^R = (\lambda^{-1} - 2329.66\ \mathrm{cm}^{-1})^{-1}$ denotes the N_2 Raman shifted wavelength and z_s is the altitude of the lidar instrument. The subscripts $\|$ and $\perp$ denote the aligned- and cross-polarized component, respectively. K is determined by normalizing $R_{\|}$ to unity between 16 and 18 km as during the campaign no cloud layers were observed above 16 km. Volume depolarization δ and aerosol depolarization δ^A are defined by

$$\delta = \frac{\beta_{\perp}^{M} + \beta_{\perp}^{A}}{\beta_{\|}^{M} + \beta_{\|}^{A}} \qquad \delta^A = \frac{\beta_{\perp}^{A}}{\beta_{\|}^{A}} = \frac{\delta - \delta^M}{R_{\|} - 1} + \delta\,. \qquad (2)$$

δ is normalized to $\delta^M = \beta_{\perp}^{M}/\beta_{\|}^{M} = 0.014$ between 16 and 18 km [*Young*, 1980]. The measurement errors of $R_{\|}$ and δ are typically less than 3% at altitudes below 16 km. We obtain the optical depth τ between altitudes z_b and z_t from the inelastic return signals $P(z,\lambda^R)$ by

$$\tau(z_b, z_t, \lambda, \lambda^R) \;=\; \frac{1}{2}\,\ln\left(\frac{P(z_b,\lambda^R)\,(z_b - z_s)^2}{P(z_t,\lambda^R)\,(z_t - z_s)^2}\,\frac{N(z_t)}{N(z_b)}\right) \qquad (3)$$

$$-\frac{1}{2}\int_{z_b}^{z_t} dz\,(\alpha^M(\lambda)+\alpha^M(\lambda^R))$$

where $N(z)$ denotes the molecular number density and is obtained from daily aerological balloon soundings aboard "POLARSTERN". (Strictly, τ is the arithmetic mean of optical depths at λ and λ^R.) As τ is typically much smaller than unity we assume that contributions from multiple scattering processes can be ignored.

3. Results and discussion

Night-time lidar measurements were performed between 35°N and 45°S latitude and 25°W and 30°W longitude. However, the following discussion is restricted to the subtropical and tropical observations. The observations took place on 11 nights between October 18 and October 31, 1996; total measurement time was 57 hours. The analysis is based on the measurements of $R_{||}$ and δ at 355 and 532 nm between 8 and 16 km altitude.

Figure 1 summarizes the measurement of October 27/28 in terms of $R_{||}$, δ, and τ at 532 nm. Figure 1 shows several characteristic features of tropical cirrus clouds which we observed throughout the campaign. First, the clouds exhibit a high degree of temporal and spatial variability. In the vertical direction features on scales of a few tens of meters are observed. Due to the relative motion between the observed clouds and the lidar instrument the temporal evolution shown in Figure 1 should be interpreted as a horizontal cross section through a cloud layer. The horizontal cloud dimensions range from few tens to several hundred kilometers. Second, several cloud layers are found regularly with several hundred meters of vertical separation. Third, the clouds are frequently found in close vicinity to the tropopause. However, no layers were observed above the tropopause. Fourth, a large fraction of the clouds are subvisual where we assume a subvisibility threshold of $\tau = 0.03$ [*Sassen et al.*, 1989]. However, the horizontal and vertical extent of these subvisual clouds can still accurately be mapped

Figure 1.

by the depolarization detection channel. **Figure 2.**

The analysis of histogram functions shown in Figure 2 provides information on the occurrence probability of subvisual cirrus clouds. The distribution function of optical depth at 532 nm is given in Figure 2a. As the error of τ is on the order of several 10^{-3} values less than 0.001 are not shown. The middle (right) panel shows the frequency of occurrence of the maximum value of δ ($R_{||}$) between 8–16 km for $\tau < 0.03$, i.e. during clear sky and subvisual cirrus conditions.

If clouds are present values of $\delta^{\max}$ between 0.1 and 0.3 are observed most often as can be seen in Figure 2b. This contrasts with the behaviour of $R_{||}^{\max}$ (Figure 2c). For subvisual we find cirrus $R_{||}^{\max} \approx 2$ in most cases, layers with $R_{||}^{\max} > 10$ are found only rarely. We conclude that $\delta^{\max}$ is a sensitive indicator for the presence of subvisual cirrus. In the following $\delta^{\max} > 0.02$ is taken as necessary and sufficient condition for a cirrus event.

90 observations out of 172 shown in Figure 2a indicate cirrus with $\tau \geq 0.03$. (303 observations yield $\tau < 0.001$ and are not plotted.) We find in 344 cases (72%) out of 475 observations values of $\delta^{\max}$ exceeding 0.02 indicative of the presence of cirrus. Of these 344 cirrus observations 201 (58%) are classified as subvisual. In the subtropics (23°–30°) only 32% of the observations (41 out of 127 observations) show cirrus layers; here the fraction of subvisual clouds also amounts to one-half (22 observations). We note that due to the sensitivity of the depolarization detection method our occurrence frequency of subvisual cirrus is significantly higher than the values derived by *Wang et al.* [1996] based on satellite observations. **Figure 3.**

Finally, the aerosol depolarization δ^A is derived from the observed values of $R_{||}$ and δ according to Eqn. 2. As the error of δ^A becomes arbitrarily large for $R_{||}$ close to unity data with $R_{||}(\lambda_{1,2}) < 1.15$ were removed from the data set. We find that less than 0.5% of the observed values of $\delta^A(\lambda_1)$ and $\delta^A(\lambda_2)$ are zero within the two sigma level, i.e. show the characteristics of liquid cloud particles. Despite a large variability of $R_{||}$ and

δ^A within the data set a surprisingly clear structure emerges if the parallel color ratio

$$C_{\|} = \frac{R_{\|}(\lambda_1) - 1}{R_{\|}(\lambda_2) - 1} = \frac{\beta^A_{\|}(\lambda_1)}{\beta^A_{\|}(\lambda_2)} \left(\frac{\lambda_2}{\lambda_1}\right)^k$$

is plotted against the perpendicular color ratio

$$C_{\perp} = C_{\|} \frac{\delta^A(\lambda_1)}{\delta^A(\lambda_2)} = \frac{\beta^A_{\perp}(\lambda_1)}{\beta^A_{\perp}(\lambda_2)} \left(\frac{\lambda_2}{\lambda_1}\right)^k .$$

Here, $k = -4.13$ denotes the wavelength dependence of molecular scattering [*Ciddor*, 1996]. The result, the relationship between $C_{\|}$ and $C_{\perp}$, is shown in Figure 3 for four temperature ranges.

Electromagnetic scattering theory predicts that $C_{\|,\perp} \rightarrow 1$ for particles whose dimensions are much smaller than $\lambda_{1,2}$ [e.g., *Bohren and Huffman*, 1983]. On the other hand, for particles much larger than $\lambda_{1,2}$ the geometrical optics approximation applies with $C_{\|,\perp} \rightarrow (\lambda_2/\lambda_1)^k \approx 0.2$. Inspection of Figure 3a–d shows that the "small particle location" ($C_{\|,\perp} = 1$) and the "large particle location" ($C_{\|,\perp} = 0.2$) are occupied by some fraction of data points at all temperatures. However, at the latter location the observations seem to follow $C_{\perp} = 0.2\, C_{\|}^{1/3}$. In contrast to this temperature independent features a cluster of data points suddenly appears at ($C_{\|} \approx 0.1$, $C_{\perp} \approx 0.5$–3) as temperatures drop below 240 K. We suspect that changes in ice crystal shapes and/or particle size distribution at 240 K are responsible for this abrupt change [c.f., *Heymsfield and Platt*, 1984]. The position of this second cluster moves slightly to larger $C_{\|}$ as temperatures decrease further.

In conclusion we remark that only a small fraction of the observations are clustered around the "large particle location" and the "small particle location". That is the dual wavelength measurement of $R_{\|}$ and δ^A contains information with respect to cirrus particle shape and/or size distribution for a large fraction of our observations. We are confident that our data set can be used to constrain scattering matrix calculations of nonspherical particles [e.g. *Mishchenko et al.*, 1996; *Macke*, 1993] and thereby provide further insight into the microphysical properties of tropical cirrus clouds.

Acknowledgments. The help and support by the crew of "POLARSTERN" during the ALBATROSS campaign is gratefully acknowledged. We thank R. Weller and J. Gräser for providing the radio sonde data, P. Rairoux for stimulating discussions, and two anonymous reviewers for helpful comments on an earlier version of this paper. We gratefully acknowledge financial support for the MARL instrument by Deutsche Bundesstiftung Umwelt, Germany. G.B. thanks the National Research Council for the award of an associateship. Part of the work described here was performed at the Jet Propulsion Laboratory, California Institute of Technology, through an agreement with the National Aeronautics and Space Administration. Contribution 1245 of the Alfred Wegener Institute.

References

Bohren, C. F., and D. R. Huffman, *Absorption and scattering of light by small particles*, John Wiley & Sons, New York, 1983.

Borrmann, S., S. Solomon, J. E. Dye, and B. Luo, The potential of cirrus clouds for heteregeneous chlorine activation, *Geophys. Res. Lett.*, *23*, (16), 2133–2136, 1996.

Ciddor, P. E., Refractive index of air: new equations for the visible and near infrared, *Appl. Opt.*, *35*, (9), 1566–1573, 1996.

Danielsen, E. F., In situ evidence of rapid, vertical, irreversible transport of lower tropospheric air into the lower stratosphere by convective cloud turrets and by large-scale upwelling in tropical cyclones, *J. Geophys. Res.*, *98*, (D5), 8665–8681, 1993.

Heymsfield, A. J., and C. M. R. Platt, A parameterization of the particle size spectrum of ice clouds in terms of the ambient temperature and ice water content, *J. Atmos. Sci.*, *41*, 846–855, 1984.

Macke, A., Scattering of light by polyhedral ice crystals, *Appl. Opt.*, *32*, (15), 2780–2788, 1993.

Mishchenko, M. I., L. D. Travis, and D. W. Mackowski, T-matrix computations of light-scattering by nonspherical particles - A review, *J. Quant. Spectrosc. Radiat. Transfer*, *55*, (5), 535–575, 1996.

Potter, B. E., and J. R. Holton, The role of monsoon convection in the dehydration of the lower tropical stratosphere, *J. Atmos. Sci.*, *52*, (8), 1034–1050, 1995.

Prabhakara, C., R. S. Fraser, G. Dalu, M. C. Wu, R. J. Curran, and T. Styles, Thin cirrus clouds: Seasonal distribution over oceans deduced from Nimbus-4 IRIS, *J. Appl. Meteorol.*, *27*, 379–399, 1988.

Sassen, K., M. K. Griffin, and G. C. Dodd, Optical scattering and microphysical properties of subvisual cirrus clouds, and climatic implications, *J. Appl. Meteorol.*, *28*, 91–98, 1989.

Schäfer, H.-J., O. Schrems, G. Beyerle, B. Hofer, W. Mildner, F. A. Theopold, W. Lahmann, C. Weitkamp, and M. Steinbach, A modular and mobile multi-purpose lidar system

for observation of tropospheric and stratospheric aerosols, *SPIE EurOpto series*, *2581*, 128–136, 1995.

Solomon, S., S. Borrmann, R. R. Garcia, R. Portmann, L. Thomason, L. R. Poole, D. Winker, and M. P. McCormick, Heterogeneous chlorine chemistry in the tropopause region, *J. Geophys. Res.*, *102*, (D17), 21411–21429, 1997.

Stephens, G. L., S. C. Tsay, P. W. Stackhouse, and P. J. Flatau, The relevance of the micro-physical and radiative properties of cirrus clouds to climate and climate feedback, *J. Atmos. Sci.*, *47*, 1742–1753, 1990.

Wang, P.-H., M. P. McCormick, L. R. Poole, W. P. Chu, G. K. Yue, G. S. Kent, and K. M. Skeens, Tropical high cloud characteristics derived from SAGE II extinction measurements, *Atmospheric Research*, *34*, 53–83, 1994.

Wang, P.-H., P. Minnis, M. P. McCormick, G. S. Kent, and K. M. Skeens, A 6-year climatology of cloud occurrence frequency from Stratospheric Aerosol and Gas Experiment II observations (1985–1990), *J. Geophys. Res.*, *101*, (D23), 29407–29429, 1996.

Young, A. T., Revised depolarization correction for atmospheric extinction, *Appl. Opt.*, *19*, (20), 3427–3428, 1980.

G. Beyerle and I. S. McDermid, Table Mountain Facility, Jet Propulsion Laboratory, California Institute of Technology, P.O.B. 367, Wrightwood, CA 92397. (e-mail: beyerle@tmf.jpl.nasa.gov; mcdermid@tmf.jpl.nasa.gov)

J. Schäfer, Forschungszentrum Jülich GmbH, ICG3, D-52425 Jülich, Germany (e-mail: h.-j.schaefer@fz-juelich.de)

O. Schrems, Alfred Wegener Institute, P.O.B. 120 161, D-27515 Bremerhaven, Germany. (e-mail: oschrems@awi-bremerhaven.de)

R. Neuber, Alfred Wegener Institute, P.O.B. 600 149, D-14401 Potsdam, Germany. (e-mail: neuber@awi-potsdam.de)

Received XXX; revised XXX; accepted XXX.

To appear in the *Geophysical Research Letters*, 1997.

This manuscript was prepared with AGU's LaTeX macros v4, with the extension package 'AGU++' by P. W. Daly, version 1.5d from 1997/04/28.

Figure Captions

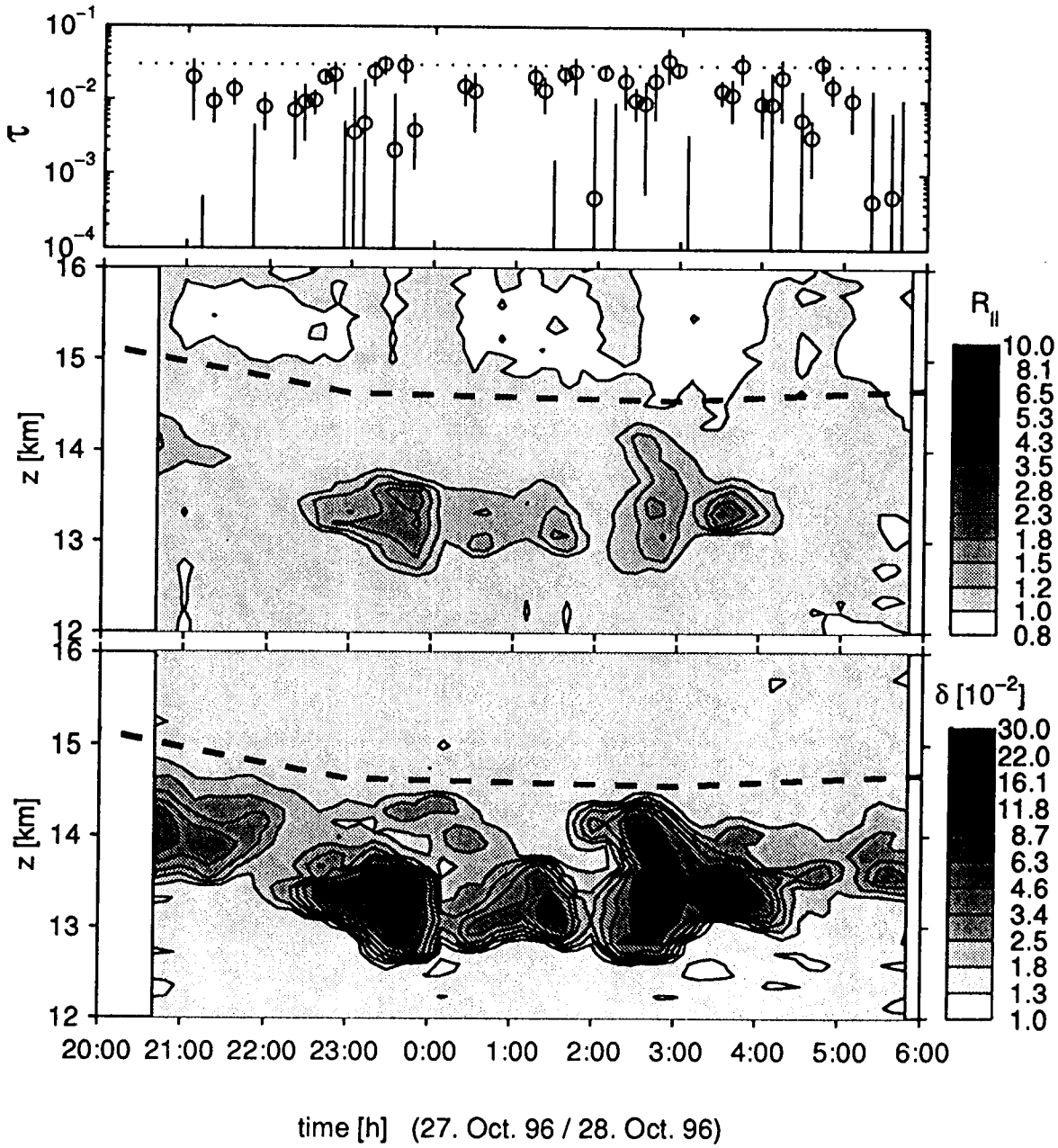

Figure 1. Temporal development of backscatter ratio (middle) and volume depolarization (bottom) at 532 nm. The tropopause altitude as interpolated from radio sondes is marked by dashed lines. (The sondes were launched at 10/27 12^{00} h, 10/27 23^{00} h, 10/28 3^{00} h, and 10/28 12^{00} h.) The top panel shows the corresponding optical depth between 8 and 12 km. The dotted line indicates the subvisibility threshold $\tau = 0.03$ classifying almost all measurements of this night as subvisual cirrus.

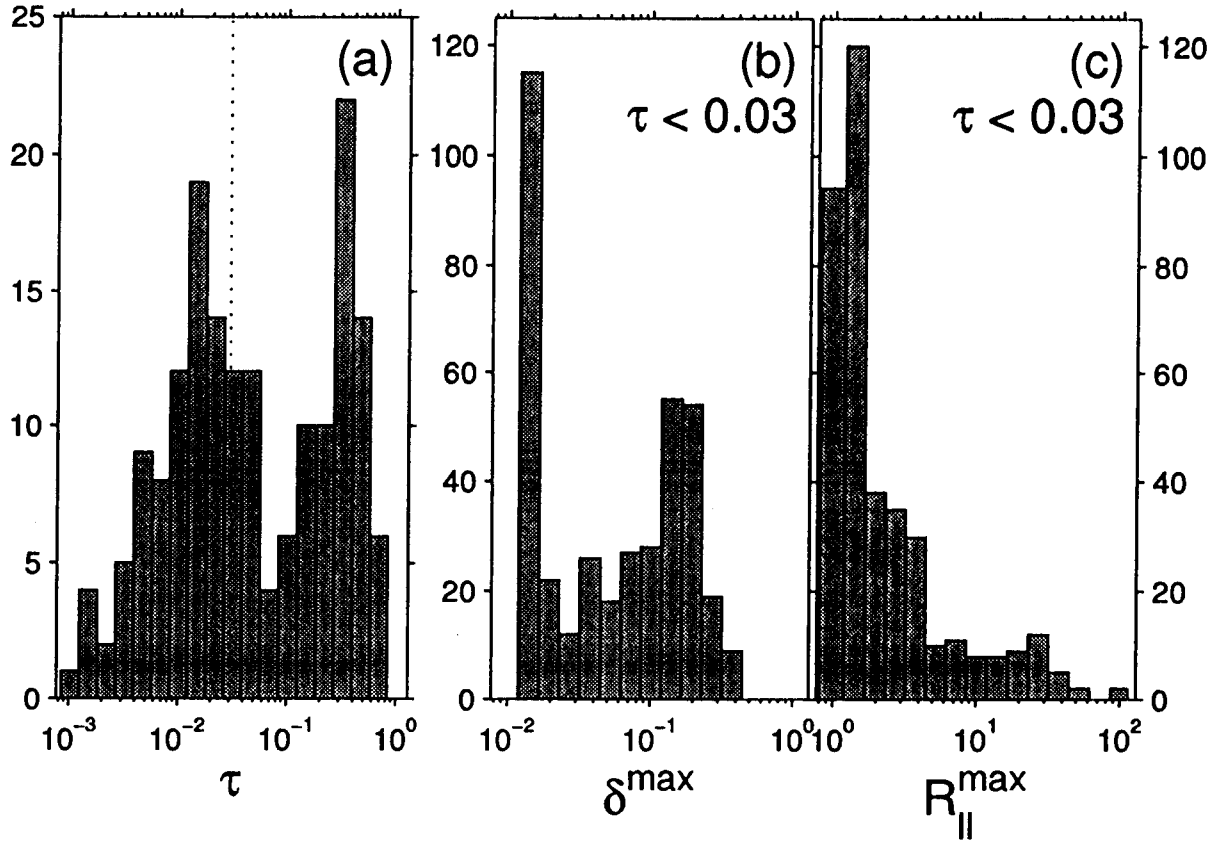

Figure 2. Histograms of the occurrence distribution of optical depth (left panel), of maximum volume depolarizations and maximum backscatter ratios within subvisual cirrus (middle and right panel) at 532 nm (23.5°N–23.5°S). τ is calculated for the altitude range 8–16 km, the vertical dotted line (left panel) indicates the subvisibility threshold $\tau = 0.03$.

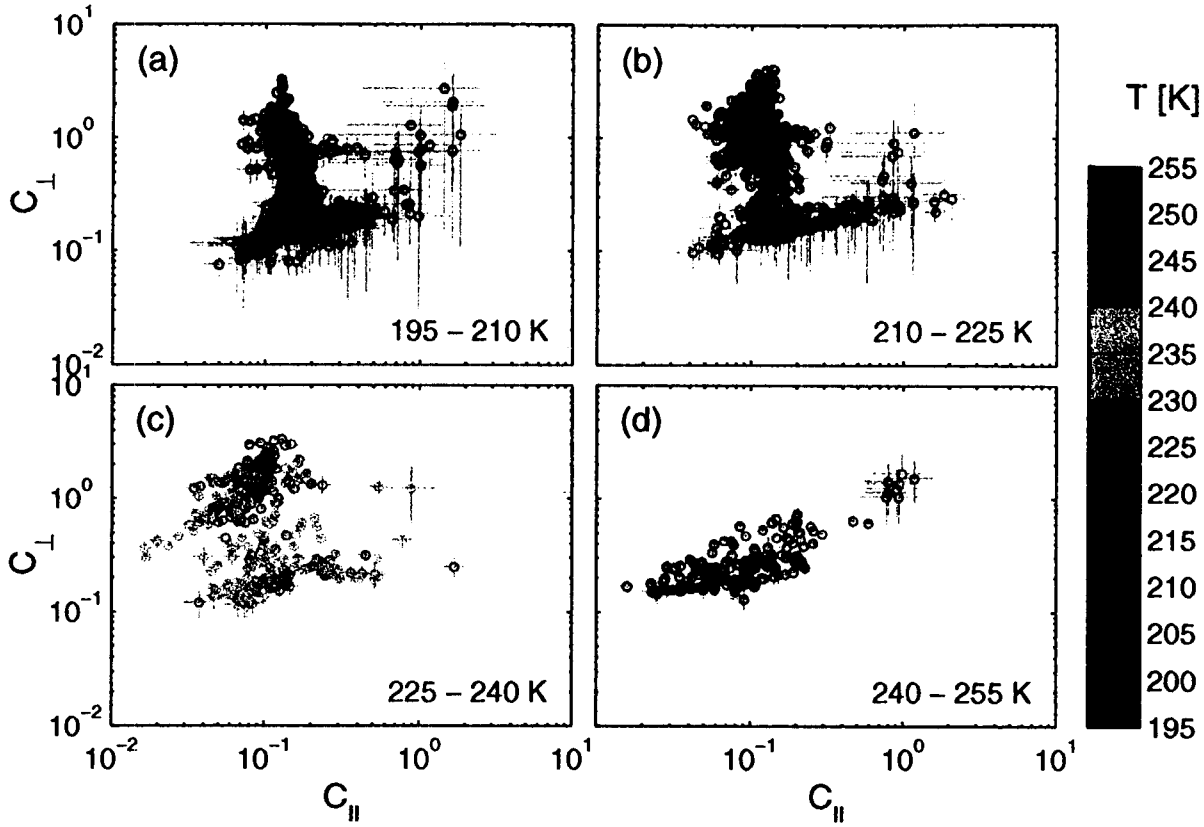

Figure 3. The relationship between the parallel color ratio $C^{||}$ and the perpendicular color ratio $C^{\perp}$ derived from the lidar observations (23.5°N–23.5°S). The individual plots show the relationship for temperature ranges of 195–210 K (a), 210–225 K (b), 225–240 K (c), and 240–255 K (d).